Chemical Engineering Journal 468 (2023) 143468

Contents lists available at ScienceDirect

Chemical Engineering Journal

journal homepage: www.elsevier.com/locate/cej

Nitration of *o*-xylene in the microreactor: Reaction kinetics and process intensification

Shuai Guo, Le-wu Zhan *, Bin-dong Li *

College of Chemical Engineering, Nanjing University of Science and Technology, Nanjing 210094, China

ARTICLE INFO

Keywords:
Nitration
Microreactor
Kinetics
Mass transfer

ABSTRACT

Nitration reactions are extensively studied in organic synthesis despite their notorious dangers, high reaction rates, and heterogeneous reaction systems. To date, most industrial nitration reactions rely on conventional batch reactors characterized by low mass transfer rates and limited reaction conditions. In contrast, microreactors represent a valuable technology for intensifying such nitration reactions. In this work, we established a continuous flow system of *o*-xylene nitration and determined the kinetics and mass transfer. The effects of mixing performance, nitric acid concentration, molar ratio, reaction temperature, and residence time on the process safety were investigated separately. The experimental data is supported by dimensionless number calculations, providing a more comprehensive understanding of the nitration reaction's transport and reaction performance in a heart-shaped microreactor. Remarkably, the residence time of the heart-shaped microreactor was reduced by an order of magnitude, while the volumetric mass transfer coefficient was improved by several orders of magnitude compared to conventional stirred tank reactors. Moreover, the spent nitric acid could be efficiently recovered and reused after concentration, further enhancing the sustainability and cost-effectiveness of the process. Our findings demonstrate the significant potential of microreactors for intensifying nitration reactions and paving the way for the design and optimization of more efficient and safer synthetic processes.

1. Introduction

Nitroaromatic compounds are widely used as intermediates to prepare dyes, explosives, and pharmaceuticals and are integral to organic synthesis [1,2]. The most economical nitric acid is usually selected as the nitration agent for industrial aromatic compound nitration reactions and is usually used in the presence of a strong acid catalyst [3]. However, the conventional nitration method suffers from drawbacks such as large amounts of spent acid, equipment corrosion, low product selectivity, multiple nitration and oxidation side reactions, and prolonged reaction time. These issues can be attributed to the high exothermic heat, fast reaction rate, and large sulfuric acid consumption of the nitration reaction [4–6]. Therefore, the nitration reaction process often occurs in thermal runaway, resulting in a decrease in product quality and even causing an explosion. Therefore, nitration reactions are regarded as one of the most hazardous reactions. [7,8].

Nitro-*o*-xylenes are the key raw material for the synthesis of pharmaceuticals and pesticides, including riboflavin, herbicide pendimethalin, and cardiovascular drug tolvaptan [9–11]. As a result, the nitration reaction of *o*-xylene has received significant attention in the literature, as evidenced by the vast number of studies summarized in Table 1 [12–19]. Despite more than seven decades of research, the development of effective and sustainable methods for the nitration of *o*-xylene remains a critical area of investigation. Attempts to address this challenge have led to the emergence of novel nitration agents, such as polyphosphoric acid, H-Y zeolite catalyst, carbon molecular sieve, natural kaolinite clay, and sodium dodecyl sulfate. Although these methods have demonstrated high selectivity by using fuming nitric acid as a nitration agent and replacing waste sulfuric acid, they are time-consuming (12 to 24 h) and unsuitable for industrial-scale production. Microreactor technology offers a new approach to enhancing the efficiency of the chemical synthesis process through its high specific surface area and small reaction volume, which boost heat and mass transfer in liquid–liquid systems. [20–22]. Microreactor technology has been proven to be an effective approach for nitration reactions in numerous studies. Sharma et al. reported continuous-flow nitration of *o*-xylene. The effects of fuming nitric acid and mixed acids as nitration agents on the nitration reaction of *o*-xylene were investigated separately in a tubular reactor and the feasibility of process scale-up was analyzed. The findings indicated that the content of poly-nitro impurities was higher when sulfuric acid was present, while the yield of 1,2-dimethyl-4-

* Corresponding authors.
E-mail addresses: zhanlewu@sina.com (L.-w. Zhan), libindong@njust.edu.cn (B.-d. Li).

https://doi.org/10.1016/j.cej.2023.143468
Received 7 December 2022; Received in revised form 5 May 2023; Accepted 9 May 2023
Available online 19 May 2023

Nomenclature

u	Superficial velocity, $m{\cdot}s^{-1}$
Q	Volumetric feed flow rate, $mL{\cdot}min^{-1}$
d_H	Hydraulic diameter of the microchannel inlet, m
q	Volumetric flow rate ratio of organic liquid to aqueous solution
V_R	Volume of the microchannel internal, mL
C_A^0	Fluid-phase inlet reactant concentration, $mol{\cdot}L^{-1}$
n_A	Amount of substance A, mol
A	Channel inlet cross-sectional area, mm^2
h	Channel height, mm
w	Channel width, mm
Re	Reynolds number
Ca	Capillary number
De	Dean number
R	Radius of curvature, mm
K_La	Volumetric mass transfer coefficient, s^{-1}
ΔC_m	Logarithmic mean concentration, $mol{\cdot}L^{-1}$
$C^*_{or.in}$	Equilibrium concentration of *o*-xylene in the nitric acid phase at the inlet, $mol{\cdot}L^{-1}$
$C_{or.in}$	Concentration of *o*-xylene in the nitric acid phase at the inlet, $mol{\cdot}L^{-1}$
x	*o*-xylene conversion, %
$\Delta_r H^\theta_m$	Standard molar reaction enthalpies of formation, $kJ{\cdot}mol^{-1}$
$\Delta_f H^\theta_m$	Standard molar enthalpy of formation, $kJ{\cdot}mol^{-1}$
ΔT_{ad}	Adiabatic temperature rise, K
Cp_m	Average specific heat capacity, $kJ{\cdot}kg^{-1}{\cdot}K^{-1}$
m	Mass of reacting substances, g
Nu	Nusselt number
Da_{II}	Second Damköhler number
t_h	characteristic heat transfer time, s
D	Dispersion coefficient, $m^2{\cdot}s^{-1}$
M_{HNO_3}	Molecular weight of HNO_3, $g{\cdot}mol^{-1}$
$M_{o-xylene}$	Molecular weight of *o*-xylene, $g{\cdot}mol^{-1}$
$V_{o-xylene}$	Molar volume of *o*-xylene at its normal boiling point, $cm^3{\cdot}mol^{-1}$
V_c	critical volume, $cm^3{\cdot}mol^{-1}$, $cm^3{\cdot}mol^{-1}$
$F^0_{o-xylene}$	Initial mass flow rate of *o*-xylene, $g{\cdot}s^{-1}$

Greek symbols

τ	Reaction time, s
τ_D	Diffusion time, s
τ_r	Characteristic reaction time, s
σ	Fluid interfacial tension, $kg{\cdot}s^{-2}$
α	Heat transfer coefficient, $W{\cdot}m^{-2}{\cdot}K^{-1}$
λ_f	Heat conductivity of the microreactor, $W{\cdot}m^{-1}{\cdot}K^{-1}$
β	Order of the reaction
ρ_M	average density of the two immiscible liquid phases, $kg{\cdot}m^{-3}$
φ	Volumetric flowrate ratio of organic liquid to total liquid
μ_M	Average viscosity of the two immiscible liquid phases, Pa·s
Φ_{HNO3}	Association factor of HNO_3
η	Space-time yield, $g{\cdot}cm^{-3}{\cdot}h^{-1}$

Subscripts

aq	Aqueous phase
or	Organic phase
in	Inlet of the reactor
out	Outlet of the reactor

Table 1
Literature on *o*-xylene nitration.

Authors	T (℃)	Nitration agent	Conversion (%)	3-NO_2 (%)[f]	4-NO_2 (%)[g]
Kobe[12]	25	HNO_3/H_2SO_4	90	58	42
Sengupta[13]	50[a]	FNA	85	–	71
Tang[14]	50	$NO_2 + BiCl_3$	71.3	14.5	56.8
Bharadwaj[15]	0	HNO_3 + Al $(H_2PO_4)_3$	87	20	80
Yadav[16]	30[b]	HNO_3	18	42	53
Wang[17]	50[c]	HNO_3/H_2SO_4	99.2	27.2	71.1
Sharma[18]	20[d]	HNO_3/H_2SO_4	99	53	39
	40[d]	FNA	80	35	45
Song[19]	100[e]	HNO_3/H_2SO_4	95.5	54.3	45.7

[a] H-Y zeolite catalyst, 115 % H_3PO_4, FNA. [b]Carbon molecular sieve and natural kaolinite clay. [c]Sodium dodecyl sulfate. [d,e]Continuous-flow nitration of *o*-xylene. [f]3-NO_2 is 1,2-dimethyl-3-nitrobenzene. [g]4-NO_2 is 1,2-dimethyl-4-nitrobenzene.

nitrobenzene was consistently lower than that of fuming nitric acid alone [18]. In another study, Song et al. successfully performed an efficient nitration process of *o*-xylene at a pilot scale using the Corning Advanced-Flow Reactor G1. The study utilized an H_2SO_4 concentration of 70 % at 100 ℃, with a molar ratio of H_2SO_4 to HNO_3 of 3 and a molar ratio of HNO_3 to *o*-xylene of 1.2, resulting in a product yield of 94.1 % and a throughput of 800 g/h. In comparison to the batch process, the study achieved a significant reduction of phenolic impurities. These findings demonstrated the efficiency and effectiveness of the Advanced-Flow Reactor G1 in enabling chemical processes at a pilot scale [19]. At present, the research on the process of *o*-xylene nitration reaction focuses on three aspects: First, classical mixed acid is utilized in batch reactors to directly react with *o*-xylene for industrial production. Secondly, the development of green chemical methods by employing various nitration agents. Thirdly, the utilization of continuous flow reactor technology enhances the fundamental safety of the nitration reaction process. In summary, the microreactor technology is effective and feasible for the intensification of the *o*-xylene nitration process and the study on the process of nitration reaction is relatively sufficient. However, the lack of theoretical studies on the nitration process of *o*-xylene and the absence of reliable methods to accurately determine kinetic data in microreactors present challenges in guiding industrial production. Therefore, there is an urgent need to improve the theoretical understanding of the process and develop a greener and more economical synthesis route. Meeting these challenges will be crucial to providing a better understanding of the parameters governing the reaction and enabling the development of more efficient and reliable ways to produce *o*-xylene.

The mixing mode of the fluid in the reactor plays an important role in determining the success of the liquid–liquid reaction. For two reaction materials to successfully react, they must first come into contact with one another at a molecular scale. Therefore, the quality of mixing and fluid flow in the reactor has a direct impact on the degree to which materials can interact [23,24]. This is particularly important in fast nitration reactions. When the micro-mixing time of the liquid phase exceeds the characteristic reaction time, poor micro-mixing can lead to a situation in which the chemical reaction occurs before the materials have been fully mixed and homogenized [25]. The study by Song et al. focuses on the influence of mixing performance on the polymerization of acrylamide in capillary microreactors. The experiment showed that while a monomer conversion of 87 % was achieved within the capillary length, the characteristic mixing time calculation indicates that the reaction process did not reach a uniform mixing state. To mitigate the

impact of inadequate mixing during polymerization, the researchers enhanced the mixing process by incorporating a premier into the reaction [26]. Yang et al. investigated the effect of advanced flow reactor mixing performance on the continuous production of nanomaterials. The results have shown that the variation of the flow rate ratio affects the initial concentration distribution profile, resulting in different mixing properties. With increased total flow rates, micro-mixing efficiency was found to also increase and subsequently led to a narrowing of the Particle Size Distribution (PSD) of Ag NPs [27]. While there is ample evidence in the literature that microreactor systems can effectively intensify mixing and mass transfer in chemical reactions, detailed theoretical studies on how these factors impact the nitration process of *o*-xylene have yet to be conducted. Microreactor technology provides an efficient method for nitration reactions, but its effectiveness is hindered by limited liquid mixing within the reactor, which primarily relies on intermolecular diffusion to facilitate liquid–liquid heterogeneous nitration reactions. As such, there are several obstacles to overcome for the successful implementation of microreactor technology in this process [28]. Dimensionless numbers are useful to determine or compare the importance of physical or chemical processes in a system [29,30]. By considering these factors, it becomes possible to gain a better understanding of how the interaction between hydrodynamics, mass transport and reaction performance influences the nitration reaction process in microreactors. In addition, the precise temperature control performance provides a basis for revealing the characteristics and mechanism of nitration reactions. For this reason, it is necessary to study the influence of mixing and mass transfer properties on the reaction.

In this work, the effects of mixing performance and mass transfer for liquid–liquid systems intensification on the reaction process in the microreactor were systematically investigated by using the nitration reaction of *o*-xylene as a probe reaction. Firstly, the safety of the nitration process was assessed by calculating the adiabatic temperature rise. Secondly, the effects of microreactor mixing and mass transfer on the nitration reaction process, such as flow rate, residence time, reaction temperature, and molar rate were investigated in detail. Finally, a kinetic model was established to guide the nitration process of *o*-xylene in the microreactor.

2. Experimental section

2.1. Material preparation

All reagents (*o*-xylene ≥ 99 %; Sulfuric acid ≥ 98 %; Fuming nitric acid ≥ 98 %; dichloromethane ≥ 99 %; NaOH; Na_2SO_4) purchased from Shanghai Aladdin Bio-Chem Technology Co., Ltd. All aqueous solutions used in the experiments were deionized water. Different concentrations of nitric acid and sulfuric acid were obtained by dilution with deionized water. All chemicals were used without further purification.

2.2. Micro-reaction system

A schematic diagram of the micro-reaction system set-up for the *o*-xylene nitration reaction is shown in Fig. 1. The micro-reaction system is made up of four primary units: feed unit, reaction unit, quenching unit, and separation unit. The *o*-xylene solution and nitric acid solution in the feeding unit were introduced into the microchannel reaction unit as the dispersed phase and the continuous phase, respectively, using two high-precision metering pumps (Sanotac-MPF0502C, Shanghai, China; flow rate, 0–100.00 mL·min^{-1}; pressure range, 0–4 MPa). Subsequently, the *o*-xylene and nitric acid solutions passed through the pre-cooling coil (PTFE, inner diameter: 1 mm) into the microreactor for rapid mixing and reaction, respectively. The reaction unit consisted of a set of microchannel plates with a heart cell structure, as shown in Fig. 2 (Shandong Weijing Chemical Technology Co., Ltd.; total internal volume: 30 mL; material: Hastelloy). The temperature control of the reaction unit was maintained by high and low-temperature circulation equipment (GDSZ-50L/-30 °C, Zhengzhou Ruihan Instrument Co., Ltd., China) to keep the temperature of the reaction process stable. The residence time was obtained by varying the flow rate or increasing the number of channel plates. After the reaction, an aqueous solution was introduced at the outlet of the microchannel plate for the quenching reaction by a high-precision metering pump, and the entire quenching unit (PTFE, length: 2 m; inner diameter: 1 mm) was submerged in an ice-water bath. Finally, the quenched mixture enters the separation unit for static separation. The organic phase is located in the upper layer containing nitrocompounds and *o*-xylene, and the lower layer is the aqueous phase of nitric acid. The organic layer is washed with NaOH aqueous solution and deionized water, separately, and then dried with Na_2SO_4 to obtain the

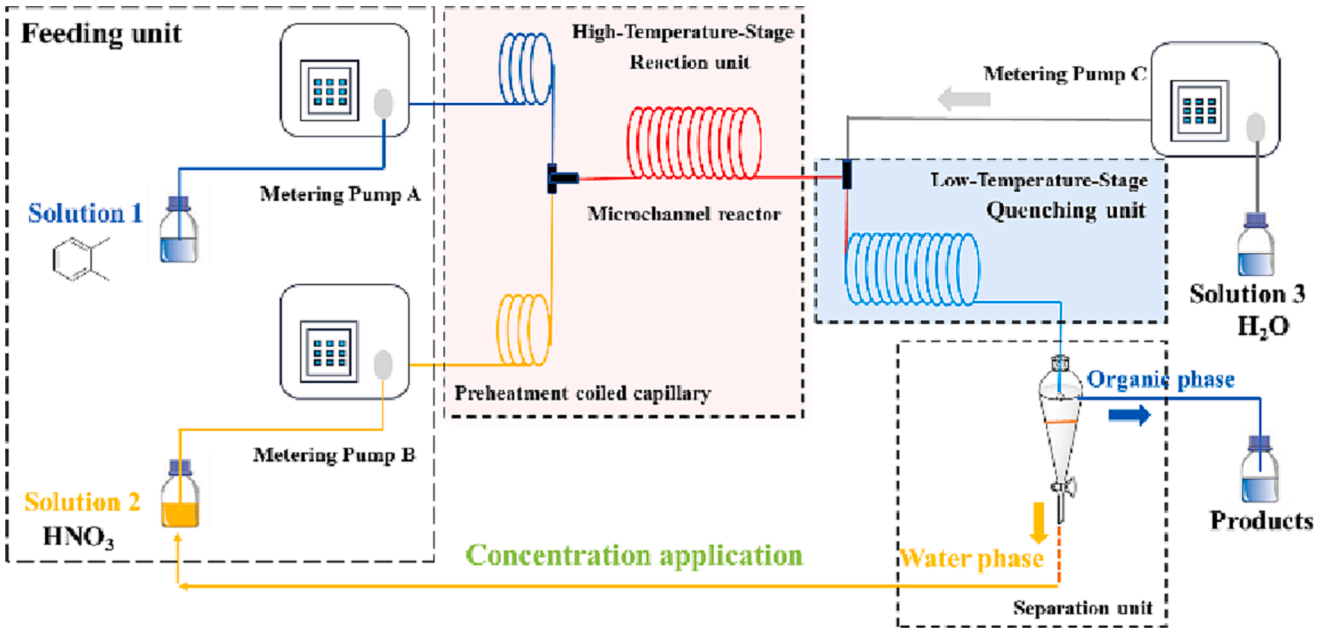

Fig. 1. Schematic diagram of the experimental set-up.

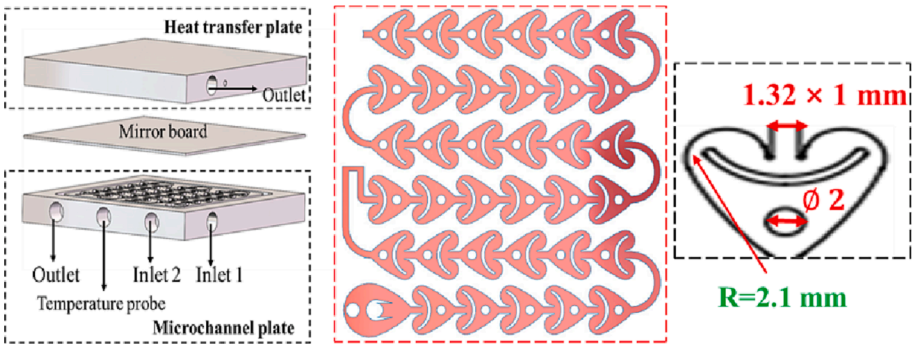

Fig. 2. Schematic diagram of the microchannel structure.

products. The aqueous phase is concentrated to obtain a concentration of 82–84 % nitric acid as shown in Fig. 3.

2.3. Sample analyses

The organic phase mixtures were diluted with dichloromethane solution and analyzed by gas chromatography (Bruker 450-GC; column: AESE-54; 30 m × 0.32 mm × 0.5 μm). The column temperature was maintained at 70 ℃ for 2 min, then increased to 150 ℃ by 15 ℃·min^{-1}, and held for 2 min, then increased to 300 °C by 20 °C·min^{-1}, and then held for 3 min. The injector and FID detector temperatures were set to 280 ℃ and 300 ℃. The nitrogen flow rate as the carrier gas was 1.0 mL·min^{-1} with a split ratio of 30:1. Calculated product concentration using the area normalization method.

2.4. Definitions of relevant parameters

The superficial velocity of HNO_3 (u_{aq}), superficial velocity of *o*-xylene (u_{or}), the O/W ratio q (volumetric flow rate ratio of *o*-xylene to HNO_3) in the experiment is defined as follows:

$$u_{aq} = \frac{4Q_{aq}}{\pi d_H^2} \tag{1}$$

$$u_{or} = \frac{4Q_{or}}{\pi d_H^2} \tag{2}$$

$$q = \frac{Q_{or}}{Q_{aq}} \tag{3}$$

The residence time (τ) is calculated by the volume of the channel (V_R) and the volumetric flow rates of the aqueous phase (Q_{aq}) and organic phase (Q_{or}):

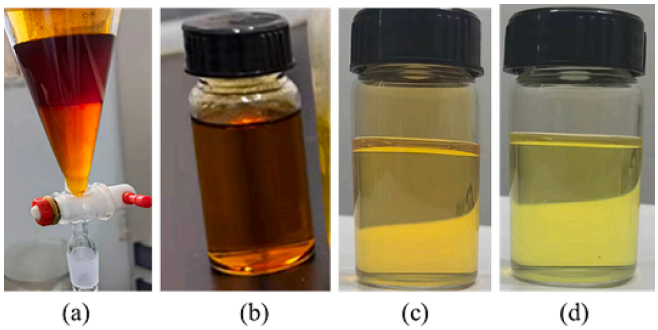

Fig. 3. Experimental diagram of spent nitric acid concentration in the separation unit. (a) Separation unit (b) Spent nitric acid (c) Concentrated nitric acid (d) Fuming nitric acid.

$$\tau = \frac{V_R}{Q_{or} + Q_{aq}} \tag{4}$$

$$C_A^0 = \frac{n_A}{Q_{or} + Q_{aq}} \tag{5}$$

$$d_H = \frac{4A}{2(h + w)} \tag{6}$$

$$\rho_M = \left(\frac{\varphi_{or}}{\rho_{or}} + \frac{1 - \varphi_{or}}{\rho_{aq}}\right)^{-1} \tag{7}$$

$$\mu_M = \left(\frac{\varphi_{or}}{\mu_{or}} + \frac{1 - \varphi_{or}}{\mu_{aq}}\right)^{-1} \tag{8}$$

$$\varphi = \frac{Q_{or}}{Q_{or} + Q_{aq}} \tag{9}$$

where C_A^0, ρ_M, μ_M, φ and n_A, are the fluid-phase inlet reactant concentration, the average density of the two immiscible liquid phases, the average viscosity of the two immiscible liquid phases, the volume fraction, and the amount of substance. d_H is equivalent diameter of the microchannel inlet, 1.13 × 10^{-3} m; V_R is microchannel total internal volume, 30 mL. The fluid properties of *o*-xylene and nitric acid parameters were presented in Table 2.

The dimensionless number of Reynolds number (*Re*), Capillary number (*Ca*), and Dean number (*De*) describing the flow behavior and mass transfer behavior of the two-phase liquid in the microchannel are expressed as follows [31]:

$$Re = \frac{\rho_M d_H u_M}{\mu_M} \tag{10}$$

$$Ca = \frac{\mu_M u_M}{\sigma} \tag{11}$$

$$De = Re\sqrt{\frac{d_H}{2R}} \tag{12}$$

In this work, the ranges of dimensionless numbers are shown Table 3.

Table 2
Fluid Properties of *o*-xylene and nitric acid at 20 °C [19].

Fluid	Density (kg·m^{-3})	Viscosity (Pa·s)	Specific Heat Capacity (kJ·kg^{-1}·K^{-1})
o-xylene	879	0.92 × 10^{-3}	1.26
Nitric acid	1500	0.89 × 10^{-3}	2

Table 3
Dimensionless numbers values of the experiment.

Dimensionless numbers	Value ranges
Re	212–1276
$Ca \times 10^2$	0.4–2.2
De	119–715

2.5. Volumetric mass transfer coefficient

In order to understand the mass transfer performance of the microreactor, a mathematical model for calculating the volumetric mass transfer coefficient was established. The mass balance of the *o*-xylene nitration reaction in the microreactor can be expressed as Eq. (13) [32,33].

$$Q_{or}(C_{or.out} - C_{or.in}) = K_L a V_R \Delta C_m \tag{13}$$

where ΔC_m is expressed as follows Eq. (14).

$$\Delta C_m = \frac{(C^*_{or.in} + C_{or.in}) - (C^*_{or.out} + C_{or.out})}{\ln(\frac{C^*_{or.in} - C_{or.in}}{C^*_{or.out} - C_{or.out}})} \tag{14}$$

nitration is a rapid reaction, so $C^*_{or.in} = C^*_{or.out} = 0$. From Eq. (13) and Eq. (14), the volumetric mass transfer coefficient $K_L a$ is expressed as follows Eq. (15).

$$K_L a = \frac{Q_{or}}{V_R} \ln(\frac{C_{or.in}}{C_{or.out}}) \tag{15}$$

Integrating Eq. (9) and Eq. (15), the relationship between *o*-xylene concentration and residence time can be deduced in Eq. (16).

$$K_L a = \frac{\varphi}{\tau} \ln(\frac{C_{or.in}}{C_{or.out}}) \tag{16}$$

Replacing the concentration with the conversion can obtain Eq. (17).

$$K_L a \tau = \varphi \ln(\frac{1}{1-x}) \tag{17}$$

3. Results and discussion

3.1. Safety assessment of the nitration reaction process in the microreactor

As the temperature is a key factor in the nitration reaction process, it is critical to evaluate potential safety hazards associated with it. Temperature increases can cause poly-nitro compounds or oxidative side reactions, and even thermal runaway events [34]. On this basis, it is necessary to conduct a safety evaluation of the nitration reaction process. First, a preliminary experiment was carried out on the nitration of *o*-xylene in the microreactor with fuming nitric acid at 283–323 K (Scheme 1). The experimental results are listed in Table 4. The experimental results show that the mononitration reaction starts at 283 K and the poly-nitration reaction starts at about 313 K, which is consistent with existing literature [18]. Aiming to gain a better understanding of the reaction hazards, the adiabatic temperature rise was calculated. The exothermic heat of the *o*-xylene mononitration reaction was estimated by empirical equation (Eq. (18), and then the data under adiabatic conditions were obtained by classical Eq.19 [35,36].

$$\Delta_r H^\theta_m = \Delta_f H^\theta_m(C_8H_9NO_2) + \Delta_f H^\theta_m(H_2O) - \Delta_f H^\theta_m(C_8H_{10}) - \Delta_f H^\theta_m(HNO_3) = -97\ kJ{\cdot}mol^{-1} \tag{18}$$

$$\Delta T_{ad} = \frac{n\Delta H}{mCp_m} = 284\ K \tag{19}$$

Based on the calculations conducted, it is clear that given the process

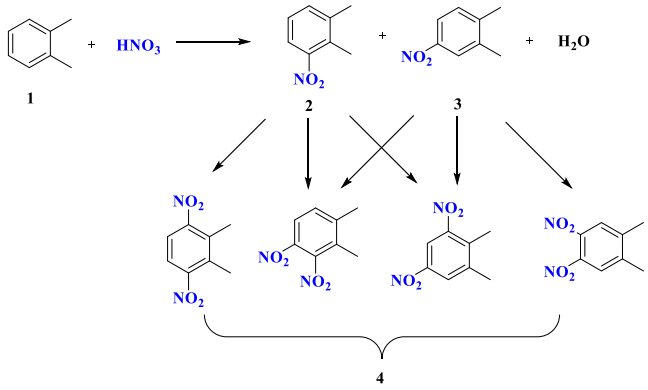

Scheme 1. Nitration of fuming nitric acid with *o*-xylene. (1) *o*-xylene (2) 1,2-dimethyl-3-nitrobenzene (3) 1,2-dimethyl-4-nitrobenzene (4) poly-nitro impurities.

Table 4
Nitration of fuming nitric acid with *o*-xylene.

Temperature (*K*)	*o*-xylene (%)	Mono-nitro compounds (%)	Poly-nitro impurities (%)
283	89.2	10.8	–
293	75.4	24.6	–
303	64.8	35.2	–
313	55.5	43.9	0.6
323	45.2	53.5	1.5

The molar ratio HNO3 (98 %) to o-xylene is 1, the total flow rate is 30 mL·min-1, τ is 1 min.

temperature of mononitration which is at 283 K, the poly-nitration is prone to initiate when subjected to adiabatic conditions, simultaneously triggering the decomposition of fuming nitric acid as illustrated in Fig. 4. The adiabatic circumstances surrounding the nitration reaction process pose a hazardous outcome, thus emphasizing the need for a detailed heat transfer analysis for the nitration reaction in the microreactor.

The Nusselt number for a fully-developed laminar flow in a circular pipe under constant temperature boundary conditions is 3.66 [37]. The constant value for other channel forms may differ and, in the secondary-flow regime, the Nusselt number increases with the *Re*. In this work, the operational flow velocity range of 10–60 mL·min^{-1}, *Re* is calculated to

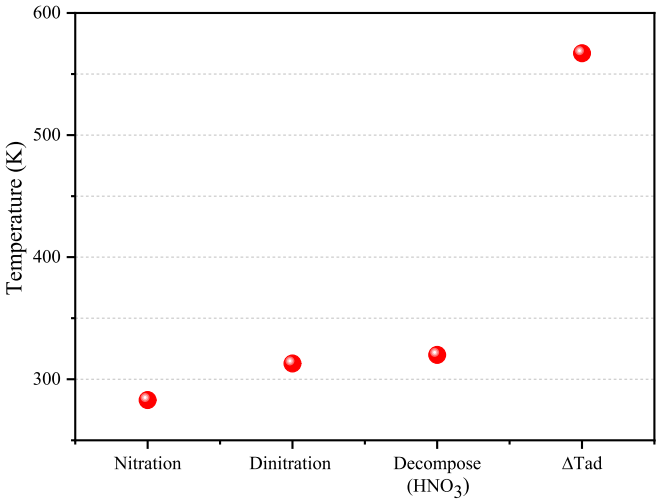

Fig. 4. Comparison between the starting temperatures and generated heats for the considered reaction: mononitration and dinitration.

be 212.67–1267, indicating that laminar flow can be obtained within the channel. For computational convenience, we assume that heat transfer can be characterized with a constant Nusslet number at a constant wall temperature.

$$Nu = \frac{\alpha d_H}{\lambda_f} = 3.66 \tag{20}$$

where α is the heat transfer coefficient, and λ_f is the heat conductivity of the microreactor, 9.8 $W{\cdot}m^{-1}{\cdot}K^{-1}$. The heat transfer characteristic time can be obtained from the heat transfer coefficient α calculated by Eq. (20) and substituted into Eq. (21) [38].

$$t_h = \frac{\rho_M Cp_m d_H}{4\alpha} \tag{21}$$

According to Kockmann et al. and Schwolow et al., it is possible to compare the characteristic reaction time with the characteristic heat transfer time to have a rough estimation. The calculated t_h is 0.02 s, which indicates that the reactants can be heated to the temperature set by the reaction in a very short time (0.02 s is negligible compared to the average residence time) [39,40]. However, it is important to note that the calculated t_h value may underestimate the actual value because of the thermal resistances that exist between the utility fluid and the process fluid. Including the thermal resistance of the metal further reduces the estimated value.

Similarly, kinetic data from the experiment can roughly estimate the distribution of reaction temperatures as shown in Fig. 5. The simulated experimental parameters are shown in Supplementary Materials Table S1. Along the axial position of the microchannel, a "hot spot" is generated near the entrance as a result of the nitration reaction taking place predominantly in the front section of the microreactor. The *o*-xylene conversion undergoes only a minor change with longer residence times, leading to a lower heat production rate, the reaction temperature subsequently decreases and becomes stable, and the temperature difference between the maximum temperature and the reaction temperature is approximately 8 K. Specifically, as the residence time increases, the temperature of the reactive mixture becomes more stable due to better heat dissipation. The results of the experiments have demonstrated that this temperature rise does not result in poly-nitration reactions.

3.2. Mixing in the nitration process in the microreactor

In microreactors, the flow rate is an important factor in controlling the flow pattern and influencing the mixing efficiency. The nitration reaction of *o*-xylene is a liquid–liquid heterogeneous reaction system, and the mixing performance directly affects the reaction process. The flow pattern for the two-phase liquids in the microreactor was calculated to be laminar flow based on the calculation of *Re*, suggesting radial diffusion as the primary mixing mechanism. The effect of flow rate on the reaction was explicitly examined in Fig. 6. Results indicate that an increase in conversion rate and a decrease in ploy-nitro impurities content are observed with increasing flow rate. When the volume flow rate exceeded 40 mL/min, the conversion trend weakened, indicating that increasing the flow rate further would not result in higher conversion. When the volume flow rate increases, the content of poly-nitro impurities in the nitration process of *o*-xylene decreases. This phenomenon is attributed to the fast and highly exothermic nature of the heterogeneous liquid–liquid reaction system. When the two-phase fluid is poorly mixed, temperature and concentration gradients are created, which can cause poly-nitration at a high molar ratio of nitric acid to *o*-xylene. The solution of *o*-xylene and nitric acid mixture first passes through the nozzle and collides with the U-shaped obstacle, which bifurcates the mixed stream into two sub-streams. The collision causes lateral movement, thus increasing the interface area for diffusion, resulting in improved mixing performance [41]. This is similar to the conclusions reported in the literature when the flow rate reaches 40 mL/min, there is a recirculation zone adjacent to near the U-shaped obstacle in the microchannel, and a Dean vortex is formed in the region of the heart-shaped bend area [42]. The centrifugal gradient in the channel cross-section generates a transverse advection or Dean vortex that enhances the mixing process by facilitating a stretching and folding mechanism and ultimately improves the mixing performance and conversion rate [43,44].

3.3. Effect of nitric acid concentration on the reaction

The concentration of nitric acid serves as a critical factor that not only affects the conversion rate of the reaction but also underlies the propensity for the occurrence of a poly-nitration reaction. The effect of nitric acid concentration on the reaction is shown in Fig. 7. It is observed that the conversion rate of the reaction increases as the nitric acid concentration goes up from 88 % to 98 %. The results showed that when the nitric acid concentration was only 98 %, the content of poly-nitro impurities was 1.8 %. Furthermore, Furthermore, by conducting linear fittings of the experimental data, it is evident that there exists a linear correlation (R^2 = 0.99) between the nitric acid concentration and the

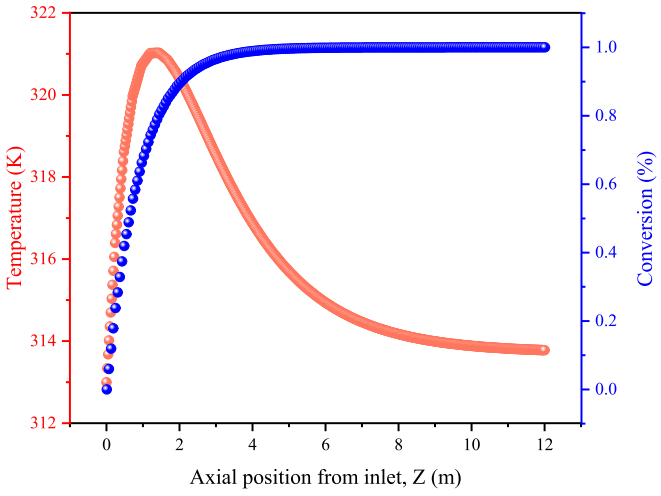

Fig. 5. Simulation of temperature profiles in the one-dimensional microchannel axial.

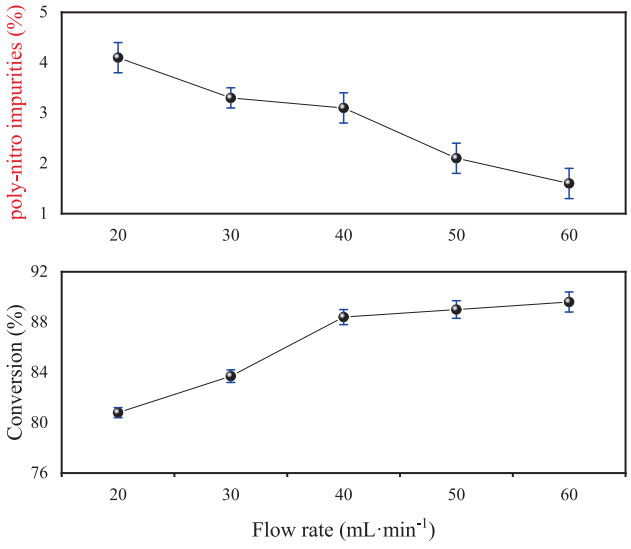

Fig. 6. Effect of flow rate on the reaction (concentration HNO_3 = 98 %, molar ratio of nitric acid to *o*-xylene = 2, temperature = 303 K, τ = 30 s).

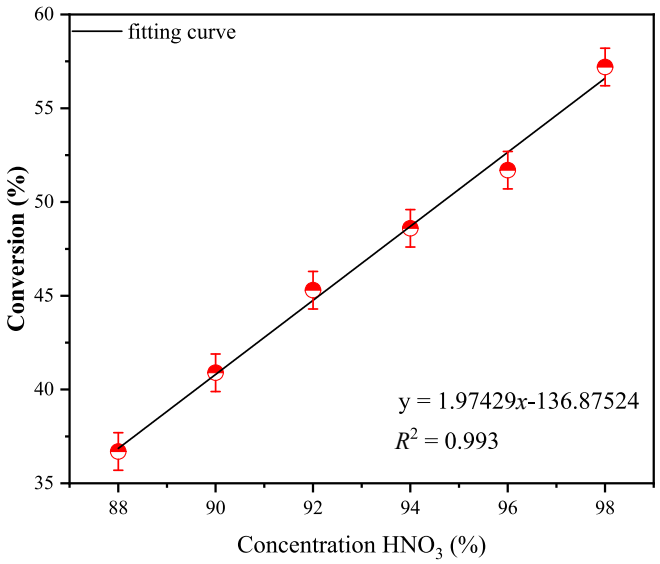

Fig. 7. Effect of nitric acid concentration on the reaction (molar ratio of nitric acid to *o*-xylene = 1.2, temperature = 313 K, total flow rate = 60 mL·min^{-1}, τ = 30 s).

conversion rate. By fitting, it was calculated that the reaction would not continue when the nitric acid concentration is below 70 %. Based on this result, this result enables one to derive the aqueous flow rate necessary for quenching. On the grounds of the result, one can safely quench the nitric acid concentration at the outlet of the microreactor by diluting it below 70 % under low-temperature conditions. This improvisation bolsters the safety of the nitration reaction, curbing the occurrence of secondary reactions.

3.4. Effect of molar rate of nitric acid to o-xylene on the reaction

Fig. 8 exhibits the effect of the molar ratio of nitric acid to *o*-xylene on the reaction. As the molar ratio increases, the NO_2^+ concentration in the system increased, and the effective chance of collision between NO_2^+ and *o*-xylene increased, increasing conversion. The experimental results demonstrate that the higher the concentration of nitric acid, the higher the conversion. This is due to the increase in the water content of concentrated nitric acid, which leads to a sharp decrease in NO_2^+ concentration and therefore the nitration capacity of nitric acid. At the same total flow rate, *q* gradually decreases with the increase of molar ratio, resulting in a gradual increase in the shear rate of the continuous phase. The droplet size of the organic phase decreases with the increase of the shear rate of the continuous phase (HNO_3), and the smaller the droplet size, the larger the interfacial area, which is conducive to the improvement of conversion rate [45]. The content of poly-nitro impurities increases with the increase of molar ratio and nitric acid concentration. When the molar ratio is less than 3, almost no poly-nitro impurities were produced at nitric acid concentrations of 90 % to 94 %. Continuing to increase the molar ratio, the impurities increase dramatically. At 303 K, the nitric acid concentrations were 94 % and 96 %, respectively, and the conversion rate was close to 100 % at a molar ratio of 4. In order to ensure product quality, the optimal nitric acid concentration was determined to be 94 %.

3.5. Kinetic model of the reaction

The conversion curves of *o*-xylene with residence time at different temperatures are shown in Fig. 9. When the temperature increases to 323 K, the conversion rate greatly improves and the reaction is completed in 9 s. The results demonstrate the high temperature

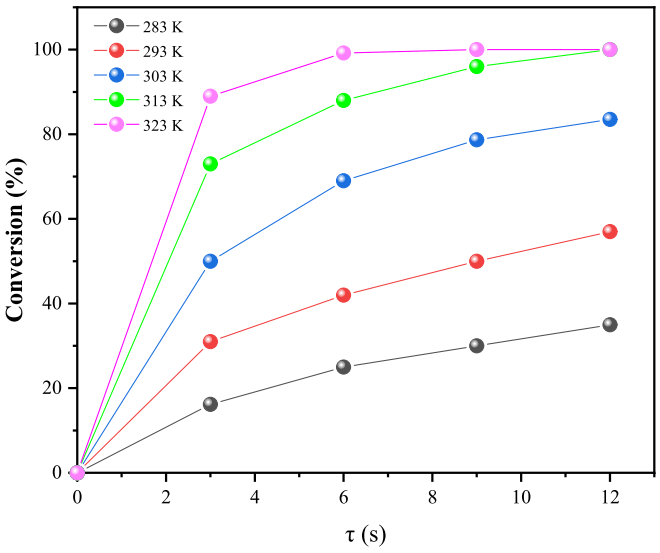

Fig. 9. The plot of conversion of *o*-xylene versus residence time at different temperatures (concentration HNO_3 = 94 %, molar ratio of nitric acid to *o*-xylene = 3.6, total flow rate = 60 mL·min^{-1}).

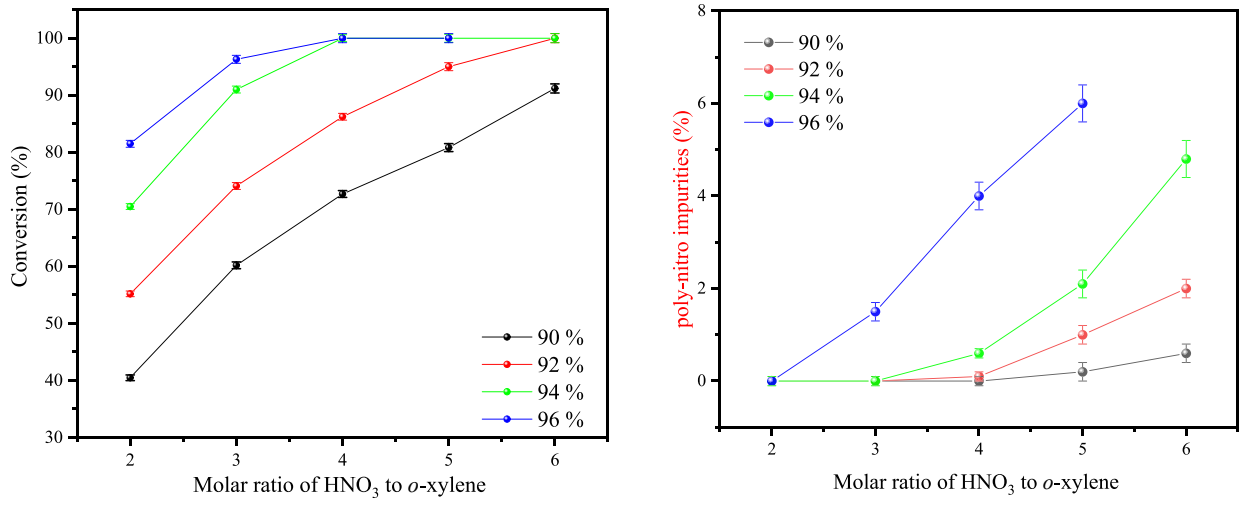

Fig. 8. Effect of molar ratio of nitric acid to *o*-xylene on the reaction. (total flow rate = 60 mL·min^{-1}, temperature = 303 K, τ = 30 s).

sensitivity of the reaction rate, which accelerates with increasing temperature.

In the experiment, when the concentration of nitric acid is 94 %, almost no poly-nitro impurities are present when the temperature is between 283 K and 323 K. Therefore, we consider that the reaction process occurs only occurs during the nitration of *o*-xylene. According to the mechanism of nitration reaction, it is known that NO_2^+ is an active substance in aromatic nitration reaction, which can be obtained by this method [46]:

$$2HNO_3 \rightarrow NO_3^- + NO_2^+ + H_2O$$

The content of NO_2^+ has a linear relationship with the concentration of fuming nitric acid. It has been demonstrated in the literature that the nitration reactions of aromatics in large amounts of fuming nitric acid follow first-order reactions [47]. Therefore, the reaction rate can be expressed as:

$$r = -\frac{dC_{o-xylene}}{d\tau} = kC_{o-xylene}C_{HNO3} \tag{22}$$

Because nitric acid was in excess in the experiment, we assume that the concentration of nitric acid is constant. Eq. (22) can be expressed as:

$$r = -\frac{dC_{o-xylene}}{d\tau} = kC_{o-xylene}C^0_{HNO3} \tag{23}$$

where k is the reaction rate constant, $C_{o-xylene}$ and C^0_{HNO3} can be replaced by the conversion rate of *o*-xylene as Eq. (24).

$$\frac{dx}{d\tau} = kC^0_{HNO3}(1-x) \tag{24}$$

Eq. (24) is integrated to obtain Eq. (25).

$$\frac{\ln(1-x)}{C^0_{HNO3}} = k\tau \tag{25}$$

Therefore, a plot of $\frac{\ln(1-x)}{C^0_{HNO3}}$ versus τ is a straight line, and k can be determined from the slope. The results are shown in Fig. 10. All the correlation coefficients R^2 are above 0.97. The results proved that there is an excellent linear relationship between $\frac{\ln(1-x)}{C^0_{HNO3}}$ and τ. This is proof that the nitration reaction of *o*-xylene with nitric acid follows a primary reaction trend, under the high excess of nitric acid.

Calculating kinetic parameters at 283–323 K and based on Arrhenius equation as Eq. (26) [48]. As shown in Fig. 11, the curve of ln$k$ versus 1/T is fitted as a straight line, and the activation energy and the pre-exponential factor can be calculated as the slope and intercept of the straight line. The value of E_a and A was found to be 53.05 kJ·mol^{-1} and 1.94 × 10^7 L·mol^{-1}·s^{-1}, respectively.

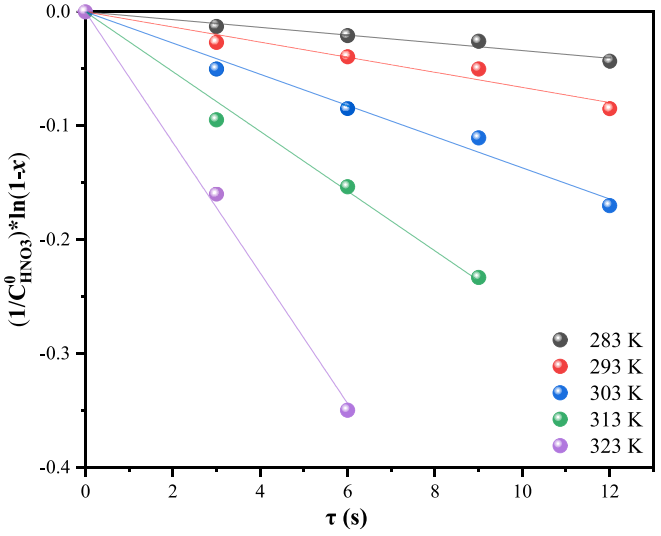

Fig. 10. Curve fitting of $\frac{\ln(1-x)}{C^0_{HNO3}}$ versus τ.

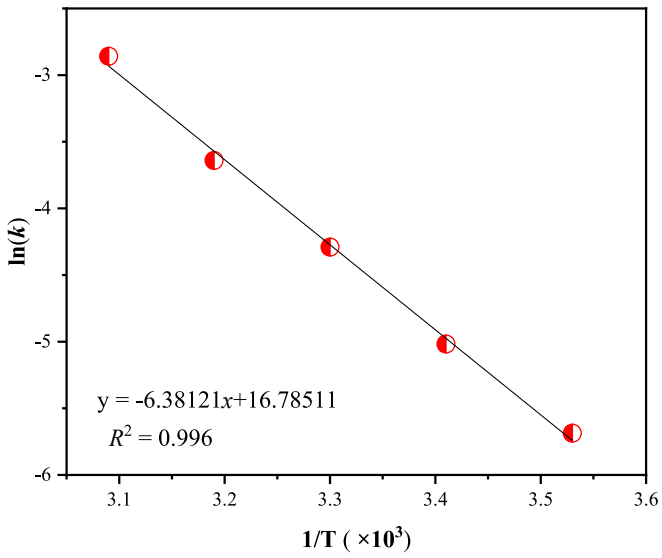

Fig. 11. The fitting of ln$k$ versus 1/T for kinetic parameters.

$$\ln k = \ln A - \frac{E_a}{RT} \tag{26}$$

where E_a and A is the activation energy and pre-exponential factor. R is the molar gas constant.

The kinetic parameters for *o*-xylene nitration obtained in this work are compared with the values reported in the literature, as shown in Table 5. The nitration rates of toluene, benzene, chlorobenzene, and nitrobenzene decreased in order. Methyl is the electron-donating group, which increases the electron cloud density of the benzene ring and speeds up the reaction rate. Chlorine and nitro are both electron-withdrawing groups, so the reaction rate is lower. The rate constant of NO_2^+ is dependent on the concentration of sulfuric acid. In this work, nitric acid was used as the nitration agent, resulting in a lower rate of NO_2^+ production compared to the mixed acid. Consequently, the reaction rate in this scenario proved to be lower than the rate constant exhibited by the reaction between toluene and the mixed acid.

3.6. Mass transfer in the nitration process in the microreactor

Fig. 12 shows the effect of the total *Re* and *q* on the volumetric mass transfer coefficient. For the same *q*, the volumetric mass transfer coefficient increases with the increase of *Re*. It can be seen from Eq. (10), *Re* is proportional to the flow velocity, and the increase in the surface flow velocity of the two-phase fluid leads to the increase of the turbulence at the interface of the two phases, which increases the volumetric mass transfer coefficient. CFD numerical simulations once again show that with the increase of *Re*, Dean vortex and recirculation zones appear in the two-phase fluid, resulting in faster renewal at the liquid–liquid two-phase interface [31]. The volumetric mass transfer coefficient increases with the decrease of *q*. This phenomenon can be explained by the reduction in dispersed phase droplet size as the continuous phase flow increases, consequently increasing the interface area and internal circulation rate [53]. According to Eq. (17), the curve of the conversion amount with residence time is a straight line through the origin, and the slope of the fit is the volumetric mass transfer coefficient, as shown in Fig. 13. The conversion rate increases with the increase of reaction temperature, and when the reaction temperature reaches 323 K, the conversion rate reaches 99.2 %, and the residence time is only 6 s. The volumetric mass transfer coefficient is 0.33219 s^{-1}.

Table 5
The measured kinetics parameters compared with literature values.

Author	Reactant	Temperature (K)	Nitrating agent	H_2SO_4 [HNO_3] (wt%)	k_{obs} at 298 K ($L{\cdot}mol^{-1}{\cdot}s^{-1}$)	*Ea* ($kJ{\cdot}mol^{-1}$)
Cox[49]	Toluene	288–308	Mixed acid	70.2	4.31	67.4
Schofield[50]	Benzene	298–317	Mixed acid	67.1	2.02×10^{-2}	75.3
Tselinskii[51]	Chlorobenzene	298–360	Nitric acid	90.5	1.13×10^{-4}	98.6
Cui[52]	Chlorobenzene	273–298	Mixed acid	95	3.64×10^{-2}	39.9
Song[48]	*p*-Nitrotoluene	288–303	Mixed acid	92	0.82	50.2
This work	*o*-xylene	283–323	Nitric acid	94	0.0102	53.05

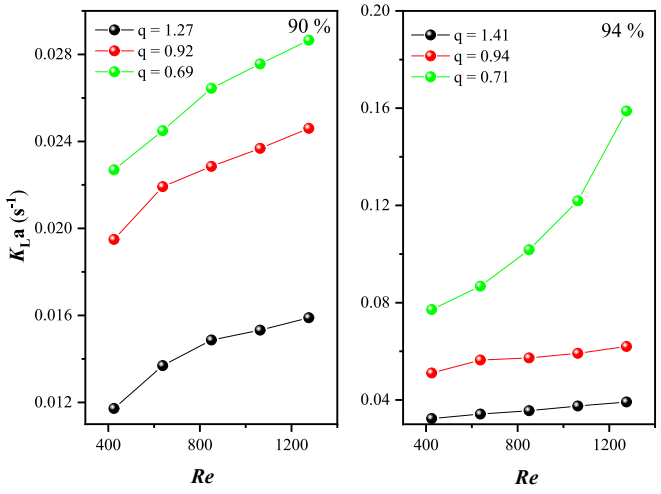

Fig. 12. Effect of *Re* and *q* on the mass transfer (temperature = 303 K).

Second Damköhler number (Da_{II}) is often used to express the time-scale ratio of the mass transfer rate to the chemical reaction rate [54]. It can be presented as follows Eq. (27):

$$Da_{II} = \frac{\tau_D}{\tau_r} \tag{27}$$

$$\tau_D = \frac{d_H^2}{4D_{o-xylene}} \tag{28}$$

$$\tau_r = \frac{1}{kc_{o-xylene}^{\beta-1}} \tag{29}$$

where τ_D is the diffusion time, τ_r is the characteristic reaction time. k is the specific reaction rate. β is the reaction order and its value is 1, and $c_{o-xylene}$ is the initial concentration of *o*-xylene [55]. $D_{o-xylene}$ can be expressed by the following equations [56]:

$$D_{o-xylene} = 7.4 \times 10^{-8} \frac{T\sqrt{\Phi_{HNO3} M_{HNO_3}}}{\mu_{HNO_3} V_{o-xylene}^{0.6}} \tag{30}$$

Therefore, increasing the reaction temperature is conducive to improving the mass transport and reaction performance of the reaction. $V_{o-xylene}$ is the molar volume of *o*-xylene at its normal boiling point, it is used to estimate as follows:

$$V_{o-xylene} = 0.285 V_c^{1.048} \tag{31}$$

According to Eq. (27), the value of *Dall* calculated in this work is in the range of $(0.16–11) \times 10^{-5}$. The value of *Da* is much less than 1, which once again indicated that the conversion was only limited by the reaction rate, and the mass transport limitation was negligible, which further confirmed the accuracy of kinetic data in the microreactor.

Table 6 presents effective interfacial areas and volumetric mass transfer coefficients in typical liquid–liquid contactors. Heart-shaped reactors and impinging jet reactors have a higher specific surface area

Table 6
Comparison of mass transfer coefficients in liquid-liquid contactors.

Contactor type	a ($m^2{\bullet}m^{-3}$)	$K_L a$(s^{-1})
Agitated contactor[a]	32–311	$(48–83) \times 10^{-3}$
Pack bed column[a]	80–450	$(3.4–5) \times 10^{-3}$
RTL extractor[a]	90–140	$(0.6–1.3) \times 10^{-3}$
Two imping jet reactors[a]	1000–3400	0.28
Heart-shaped (This work)	1000-3000[b]	0.33

[a] studies cited in ref [57]; [b]studies cited in ref [53].

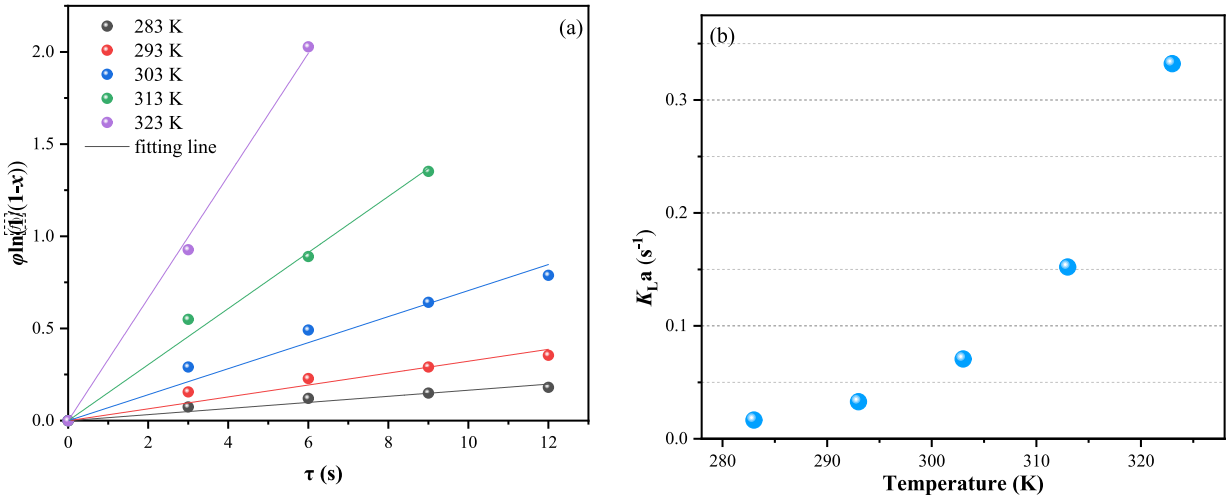

Fig. 13. Effect of temperature and residence time on the mass transfer (concentration HNO_3 = 94 %, the molar ratio of nitric acid to *o*-xylene = 3.6, total flow rate = 60 $mL{\cdot}min^{-1}$).

and therefore higher volumetric mass transfer coefficients compared to agitated contactors, packed-bed columns, and RTL extractors. Although the impinging jet reactor and heart-shaped reactor are comparable in their ability to produce specific surface area, the volumetric mass transfer coefficient in the heart-shaped reactor is higher due to the smaller droplet size and higher holding rate values. Heart-shaped reactors exhibit superior efficiency compared to other liquid–liquid contactors in generating interfacial area. This efficiency can be attributed to their unique divergent/convergent internal structure, which promotes increased interfacial area through the heart-shaped cells, requiring only energy input for pumping the fluids.

3.7. Comparison of o-xylene nitration reaction processes in the microreactor

Table 7 lists the processes reported in the literature for the nitration of *o*-xylene in the microreactor. Compared to other processes, this work shows an order of magnitude reduction in residence time and a significant advantage in product quality. This is attributed to the high mass transfer rate and the mild nitration reaction process. Space-time yield is one of the important parameters to evaluate the performance of microreactors. It is calculated by Eq. (32).

$$\eta = 3600 \times \frac{M_{nitro\ \ o-xylene}}{M_{o-xylene}} \frac{F^0_{o-xylene} X}{V_R} = 63.08\ (g{\cdot}cm^{-3}{\cdot}h^{-1}) \tag{32}$$

3.8. Analysis of utilization of spent nitric acid

The concentration of nitric acid solution after reaction quenching was about 70 %, and no impurities were detected. The concentration of spent acid after concentration treatment is about 83 %, and then it is prepared with fuming nitric acid (98 %) to make 94 % nitric acid for further reuse, without affecting the nitration reaction process. Therefore, all the spent nitric acid generated is recycled. Therefore, the new process has the advantages of environmental friendliness and high yield compared to the production processes reported in the literature.

4. Conclusions

In summary, we propose a green and efficient synthesis strategy for the nitration reaction of *o*-xylene in a continuous flow microreactor. In the microreactor with a residence time of 9 s, at 323 K, the concentration of nitric acid is 94 %, and the conversion reached 100 %. The volumetric mass transfer coefficient of the microreactor reached 0.33 s^{-1}. The superior performance of this device versus other conventional liquid–liquid contactors in terms of overall mass transfer coefficients and power consumption has been shown.

The process safety for the nitration of *o*-xylene was carefully evaluated by nitration reaction adiabatic temperature rise and the characteristic heat transfer time of the microreactor. Firstly, a kinetic model of *o*-xylene nitration in a microreactor was established, and the activation energy and pre-exponential factor of the kinetic parameters were obtained as 53.05 kJ·mol^{-1} and 1.94 × 10^7 L·mol^{-1}·s^{-1} respectively. Having obtained the kinetic parameters, a 1D dispersed plug flow model was developed. The results have shown that the high exothermic *o*-xylene nitration process in the microreactor can obtain an acceptable temperature rise of 8 K from the aspects of product quality and safety. Furthermore, according to the results of second Damköhler number, it was proved that the nitration reaction of *o*-xylene in the microreactor is kinetically controlled. At the same time, a feasible method is proposed for the reuse of waste acid generated in the nitration process. The aqueous phase after quenching is about 70 % aqueous nitric acid solution, which can be reused in proportion to the concentration of 98 % nitric acid formulated as 94 % nitric acid. This work can provide a valuable reference for the industrial production of nitration reaction of *o*-xylene.

Table 7
Comparison of *o*-xylene nitration reaction processes in the microreactor.

Authors	T (℃)	Nitration agent	τ(s)	Conversion (%)	Impurities (%)
Sharma[18]	20	HNO_3/H_2SO_4	180	100	27
	40	FNA	300	95	12
Song[19]	100	HNO_3/H_2SO_4	90	95.5	0.1
This work	50	HNO_3	9	100	0

Declaration of Competing Interest

The authors declare that they have no known competing financial interests or personal relationships that could have appeared to influence the work reported in this paper.

Data availability

No data was used for the research described in the article.

Acknowledgments

The authors would like to acknowledge the National Natural Science Foundation of China (No. 21875109) for providing funds for conducting experiments.

Appendix A. Supplementary data

Supplementary data to this article can be found online at https://doi.org/10.1016/j.cej.2023.143468.

References

[1] Y.Z. Chen, Y.C. Zhao, M. Han, C.B. Ye, M.H. Dang, G.W. Chen, Safe, efficient and selective synthesis of dinitro herbicides via a multifunctional continuous-flow microreactor: one-step dinitration with nitric acid as agent, Green Chem. 15 (2013) 91–94, https://doi.org/10.1039/c2gc36652e.
[2] R. Calvo, K. Zhang, A. Passera, D. Katayev, Facile access to nitroarenes and nitroheteroarenes using N-nitrosaccharin, Nat. Comm. 10 (2019) 3410, https://doi.org/10.1038/s41467-019-11419-y.
[3] B. Kilpatrick, M. Heller, S. Arns, Chemoselective nitration of aromatic sulfonamides with tertbutyl nitrite, Chem. Commun. 49 (2013) 514–516, https://doi.org/10.1039/c2cc37481a.
[4] J. Huang, F. Ding, P. Rojsitthisak, F.-S. He, J. Wu, Recent advances in nitro-involved radical Reactions, Org. Chem. Front. 7 (18) (2020) 2873–2898.
[5] T. Yang, X.Q. Li, S. Deng, X.T. Qi, H.J. Cong, H.G. Cheng, L.W. Shi, Q.G. Zhou, L. Zhuang, From N-H Nitration to Controllable Aromatic Mononitration and Dinitration-The Discovery of a Versatile and Powerful N-Nitropyrazole Nitrating Reagent, JACS Au. 2 (2022) 2152–2161, https://doi.org/10.1021/jacsau.2c00413.
[6] D. Russo, G. Tomaiuolo, R. Andreozzi, S. Guido, A.A. Lapkin, I.D. Somma, Heterogeneous benzaldehyde nitration in batch and continuous flow microreactor, Chem. Eng. J. 377 (2019), 120346, https://doi.org/10.1016/j.cej.2018.11.044.
[7] Z. Lan, Y.C. Lu, Continuous nitration of o-dichlorobenzene in micropacked-bed reactor: process design and modelling, J Flow Chem. 11 (2021) 171–179, https://doi.org/10.1007/s41981-020-00132-3.
[8] S. Guo, G.K. Zhu, L.W. Zhan, B.D. Li, Continuous kilogram-scale process for the synthesis strategy of 1,3,5-trimethyl-2-nitrobenzene in microreactor, Chem. Eng. Res. Des. 178 (2022) 179–188, https://doi.org/10.1016/j.cherd.2021.12.029.
[9] S.S. Neti, C.D. Poulter, Site-Selective Synthesis of 15N- and 13C- Enriched Flavin Mononucleotide Coenzyme Isotopologues, J. Org. Chem. 81 (2016) 5087–5092, https://doi.org/10.1021/acs.joc.6b00640.
[10] I. Di Somma, R. Marotta, R. Andreozzi, V. Caprio, Nitric acid decomposition kinetics in mixed acid and their use in the modeling of aromatic nitration, Chem. Eng. J. 228 (2013) 366–373, https://doi.org/10.1016/j.cej.2013.04.100.
[11] A. Corderovargas, B. Quicletsire, S. Zard, A flexible approach for the preparation of substituted benzazepines: application to the synthesis of tolvaptan, Bioorg. Med. Chem. 14 (2006) 6165–6173, https://doi.org/10.1016/j.bmc.2006.05.070.
[12] K.A. Kobe, P.W. Pritchett, Mononitration of p-xylene, Ind. Eng. Chem. 44 (1952) 1398–1401, https://doi.org/10.1021/ie50482a037.
[13] S.K. Sengupta, J.A. Schultz, K.R. Walck, D.R. Corbin, J.C. Ritter, Synthesis of 4-nitro *o*-xylene by selective nitration of *o*-xylene, Top. Catal. 55 (2012) 601–605, https://doi.org/10.1007/s11244-012-9837-8.
[14] B. Tang, S.B. Wei, X.H. Peng, Acid-catalyzed regioselective nitration of *o*-xylene to 4-nitro *o*-xylene with nitrogen dioxide: Brønsted acid versus Lewis acid, Synthetic Comm. 44 (2014) 2057–2065, https://doi.org/10.1080/00397911.2013.873468.

[15] S.K.S. Bharadwaj, M. Hussain, M.K. Kar, Chaudhuri Al(H_2PO_4)$_3$: An efficient catalyst for nitration of organic compounds with nitric acid, Catal. Comm. 9 (2008) 919–923, https://doi.org/10.1016/j.catcom.2007.09.020.
[16] G.D. Yadav, P.M. Bisht, S.V. Land, Regioselective nitration of *o*-xylene by using a novel clay-based shape-selective acid catalyst, Catal. Today. 141 (2009) 56–60, https://doi.org/10.1016/j.cattod.2008.07.019.
[17] P.C. Wang, M. Lu, J. Zhu, Y.M. Song, X.F. Xiong, Regioselective nitration of aromatics under phase-transfer catalysis conditions, Catal. Comm. 14 (2011) 42–47, https://doi.org/10.1016/j.catcom.2011.07.013.
[18] Y. Sharma, R.A. Joshi, A.A. Kulkarni, Continuous-Flow Nitration of o-xylene: Effect of Nitrating Agent and Feasibility of Tubular Reactors for Scale-Up, Org. Process Res. Dev. 19 (2015) 1138–1147, https://doi.org/10.1021/acs.oprd.5b00064.
[19] Q. Song, X.G. Lei, S. Yang, S. Wang, J.H. Wang, J.J. Chen, Y. Xiang, Q.W. Huang, Z. Y. Wang, Continuous-flow synthesis of nitro-o-xylenes: process optimization, impurity study and extension to analogues, Molecules 27 (2022) 5139, https://doi.org/10.3390/molecules27165139.
[20] X. Wang, T. Zhang, L. Lv, W.X. Tang, R.K. Gupta, S.W. Tang, Reaction performance and flow behavior of isobutane/1-butene and H_2SO_4 in the microreactor configured with the micro-mixer, Ind. Eng. Chem. Res. 61 (2022) 9122–9135, https://doi.org/10.1021/acs.iecr.2c01664.
[21] Z.F. Yan, C.C. Du, Y.B. Wang, J. Deng, G.S. Luo, Dehydrochlorination of β-chlorohydrin in continuous microflow system: Reaction kinetics and process intensification, Chem. Eng. J. 444 (2022), 136498, https://doi.org/10.1016/j.cej.2022.136498.
[22] P.L. Suryawanshi, S.P. Gumfekar, B.A. Bhanvase, S.H. Sonawane, M.S. Pimplapure, A review on microreactors: Reactor fabrication, design, and cutting-edge applications, Chem. Eng. Sci. 189 (2018) 431–448, https://doi.org/10.1016/j.ces.2018.03.026.
[23] V. Hessel, H. Löwe, F. Schönfeld, Micromixers-a review on passive and active mixing principles, Chem. Eng. Sci. 60 (2005) 2479–2501, https://doi.org/10.1016/j.ces.2004.11.033.
[24] M.A. Schneider, T. Maeder, P. Ryser, F. Stoessel, A microreactor-based system for the study of fast exothermic reactions in liquid phase: characterization of the system, Chem. Eng. J. 101 (2004) 241–250, https://doi.org/10.1016/j.cej.2003.11.005.
[25] K.D. Nagy, B. Shen, T.F. Jamison, K.F. Jensen, Mixing and dispersion in small-scale flow systems, Org. Process Res. Dev. 16 (2012) 976–981, https://doi.org/10.1021/op200349f.
[26] Y. Song, M.J. Shang, G.X. Li, Z.H. Luo, Y.H. Su, Influence of mixing performance on polymerization of acrylamide in capillary microreactors, AIChE J. 64 (2017) 1828–1840, https://doi.org/10.1002/aic.16046.
[27] M. Yang, L.N. Yang, J. Zheng, N. Hondow, R.A. Bourne, T. Bailey, G. Irons, E. Sutherland, D. Lavric, K.J. Wu, Mixing performance and continuous production of nanomaterials in an advanced-flow reactor, Chem. Eng. J. 412 (2021), 128565, https://doi.org/10.1016/j.cej.2021.128565.
[28] F.A. D'Angelo, L. Brunet, P. Cognet, M. Cabassud, Modelling and constraint optimisation of an aromatic nitration in liquid-liquid medium, Chem. Eng. J. 91 (2003) 75–84, https://doi.org/10.1016/S1385-8947(02)00139-0.
[29] Y.H. Su, G.W. Chen, Q. Yuan, Influence of hydrodynamics on liquid mixing during Taylor flow in a microchannel, AIChE J. 58 (2012) 1660–1670, https://doi.org/10.1002/aic.12698.
[30] S.T. Masoni, M. Antognoli, A. Mariotti, R. Mauri, M.V. Salvetti, C. Galletti, E. Brunazzi, Flow regimes, mixing and reaction yield of a mixture in an X-microreactor, Chem. Eng. J. 437 (2022), 135113, https://doi.org/10.1016/j.cej.2022.135113.
[31] Y. Liu, T. Zhang, L. Lv, Y.X. Chen, S.W. Tang, Mass transfer and droplet formation regime in a countercurrent mini-channel extractor, Chem. Eng. J. 402 (2020), 125383, https://doi.org/10.1016/j.cej.2020.125383.
[32] Y.B. Wang, C.C. Du, Z.F. Yan, W.H. Duan, J. Deng, G.S. Luo, Liquid-liquid flow and mass transfer characteristics in a miniaturized annular centrifugal device, Chem. Eng. J. 431 (2022), 134264, https://doi.org/10.1016/j.cej.2021.134264.
[33] F.S. Xu, L.X. Yang, G.W. Chen, Mesoscale enhancement mechanism of gas-liquid mass transfer in an ultrasonic microreactor, CIESC J. 73 (2022) 2552–2562, https://doi.org/10.11949/0438-1157.20220087.
[34] T. Westermann, L.L. Mleczko, Heat management in microreactors for fast exothermic organic syntheses-first design principles, Org. Process Res. Dev. 20 (2016) 487–494, https://doi.org/10.1021/acs.oprd.5b00205.
[35] M. Sheng, Practical Estimation techniques for determination of reaction heat, Org. Process Res. Dev. 25 (2021) 1862–1872, https://doi.org/10.1021/acs.oprd.1c00110.
[36] G.A. Weisenburger, R.W. Barnhart, J.D. Clark, D.J. Dale, M. Hawksworth, P. D. Higginson, Y. Kang, D.J. Knoechel, B.S. Moon, S.M. Shaw, G.P. Taber, D. L. Tickner, Determination of reaction heat: A comparison of measurement and estimation techniques, Org. Process Res. Dev. 11 (6) (2007) 1112–1125.
[37] S. Schwolow, J.Y. Ko, N. Kockmann, T. Röder, Enhanced heat transfer by exothermic reactions in laminar flow capillary reactors, Chem. Eng. Sci. 141 (2016) 356–362, https://doi.org/10.1016/j.ces.2015.11.022.
[38] H.L. Wei, X.B. Zhang, Z.H. Luo, Continuous synthesis of 5-oxohexanenitrile in a microreactor: from kinetic study to reactor modeling, Ind. Eng. Chem. Res. 61 (2022) 15215–15224, https://doi.org/10.1021/acs.iecr.2c02917.
[39] N. Kockmann, M. Gottsponer, B. Zimmermann, D.M. Roberge, Enabling continuous-flow chemistry in microstructured devices for pharmaceutical and fine-chemical production, Chem. Eur. J. 14 (2008) 7470–7477, https://doi.org/10.1002/chem.200800707.
[40] S. Schwolow, B. Heikenwalder, L. Abahmane, N. Kockmann, T. Röder, Kinetic and scale-up investigations of a michael addition in microreactors, Org. Process Res. Dev. 18 (2014) 1535–1544, https://doi.org/10.1021/op5002758.
[41] J.B. You, Y. Choi, S.G. Im, Influence of adjusting the inlet channel confluence angle on mixing behaviour in inertial microfluidic mixers, Microfluid Nanofluid. 21 (2017), https://doi.org/10.1007/s10404-017-1958-8.
[42] H.M. Metwally, R.M. Manglik, Enhanced heat transfer due to curvature-induced lateral vortices in laminar flows in sinusoidal corrugated-plate channels, Int. J. Heat Mass Tran. 47 (2004) 2283–2292, https://doi.org/10.1016/j.ijheatmasstransfer.2003.11.019.
[43] M.J. Nieves-Remacha, L. Yang, K.F. Jensen, Open FOAM computational fluid dynamic simulations of two-phase flow and mass transfer in an advanced-flow reactor, Ind. Eng. Chem. Res. 54 (2015) 6649–6659, https://doi.org/10.1021/acs.iecr.5b00480.
[44] K.J. Wu, V. Nappo, S. Kuhn, Hydrodynamic study of single- and two-phase flow in an advanced flow reactor, Ind. Eng. Chem. Res. 54 (2015) 7554–7564, https://doi.org/10.1021/acs.iecr.5b01444.
[45] H. Asadi-Saghandi, J. Karimi-Sabet, S. Ghorbanian, S.M.A. Moosavian, Dimensionless analysis on liquid-liquid two-phase flow patterns in a numbered-up microfluidic device, Chem. Eng. J. 429 (2022), 132428, https://doi.org/10.1016/j.cej.2021.132428.
[46] E.D. Hughes, C.K. Ingold, R.I. Reed, Kinetics of aromatic nitration: the nitronium ion, Nature. 158 (1946) 448–449, https://doi.org/10.1038/158448c0.
[47] C. Zhang, J. Zhang, G.S. Luo, Kinetic study and intensification of acetyl guaiacol nitration with nitric acid-acetic acid system in a microreactor, J Flow Chem. 6 (2016) 309–314, https://doi.org/10.1556/1846.2016.00011.
[48] J. Song, Y. Cui, L. Sheng, Y. Wang, C. Du, J. Deng, G.S. Luo, Determination of nitration kinetics of *p*-Nitrotoluene with a homogeneously continuous microflow, Chem. Eng. Sci. 247 (2022), 117041, https://doi.org/10.1016/j.ces.2021.117041.
[49] P.R. Cox, A.N. Strachan, Two phase nitration of toluene-I, Chem. Eng. Sci. 27 (1972) 457–463, https://doi.org/10.1016/0009-2509(72)87001-5.
[50] R.G. Coombes, R.B. Moodie, K. Schofield, Electrophilic aromatic substitution. Part I. The nitration of some reactive aromatic compounds in concentrated sulphuric and perchloric acids, J. Chem. Soc. B (1968) 800–804, https://doi.org/10.1039/j29680000800.
[51] E.A. Veretennikov, B.A. Lebedev, I.V. Tselinskii, Kinetics and mechanism of the nitration of chlorobenzene with nitric acid, Russ. J. Org. Chem. 37 (2001) 964–968, https://doi.org/10.1023/a:1012470315254.
[52] Y.J. Cui, J. Song, C.C. Du, J. Deng, G.S. Luo, Determination of the kinetics of chlorobenzene nitration using a homogeneously continuous microflow, AIChE. J. 68 (2022) e17564.
[53] M.J. Nieves-Remacha, A.A. Kulkarni, K.F. Jensen, Hydrodynamics of liquid-liquid dispersion in an advanced-flow reactor, Ind. Eng. Chem. Res. 51 (2012) 16251–16262, https://doi.org/10.1021/ie301821k.
[54] H. Zhang, M. Shang, Y. Song, Y. Su, Continuous synthesis of tetraalkylammonium-based ethyl sulphate ionic liquid and its kinetic study in microreactors, AIChE J. 65 (4) (2019) 1245–1255.
[55] R.L. Hartman, J.P. McMullen, K.F. Jensen, Deciding whether to go with the flow: evaluating the merits of flow reactors for synthesis, Angew. Chem. Int. Ed. 50 (2011) 7502–7519, https://doi.org/10.1002/anie.201004637.
[56] S. Guo, L.W. Zhan, G.K. Zhu, X.G. Wu, B.D. Li, Scale-up and development of synthesis 2-ethylhexyl nitrate in microreactor using the box-behnken design, Org. Process Res. Dev. 26 (2022) 174–182, https://doi.org/10.1021/acs.oprd.1c00388.
[57] M.N. Kashid, A. Renken, L. Kiwi-Minsker, Gas-liquid and liquid-liquid mass transfer in microstructured reactors, Chem. Eng. Sci. 17 (2011) 3876–3897, https://doi.org/10.1016/j.ces.2011.05.015.